Q-Band EPR and ENDOR of Low Temperature X-Irradiated β-D-Fructose Single Crystals

Gauthier C. A. M. Vanhaelewyn,[†,§,#,*] Ewald Pauwels,[‡,#] Freddy J. Callens,[†] Michel Waroquier,[‡] Einar Sagstuen,[§] and Paul F. A. E. Matthys[†]

Department of Solid State Sciences, Ghent University, Krijgslaan 281-S1, B-9000 Gent, Belgium, Center for Molecular Modeling, Ghent University, Proeftuinstraat 86, B-9000 Gent, Belgium, and Department of Physics, University of Oslo, P.O. Box 1048 Blindern, N-0316 Oslo, Norway

Received: November 16, 2005; In Final Form: December 14, 2005

β-D-Fructose single crystals were in situ X-irradiated at 80 K and measured using electron paramagnetic resonance (EPR), electron nuclear double resonance (ENDOR) and ENDOR-induced EPR (EIE) techniques at Q-band (34 GHz) microwave frequencies. The measurements revealed the presence of at least four carbon-centered radicals stable at 80 K. By means of ENDOR angular variations in the three principal crystallographic planes, six proton hyperfine coupling tensors could be determined and were assigned to four different radicals by the aid of EIE. Two of the radicals exhibit only β-proton hyperfine couplings and reveal almost identical EIE spectra. For the other two radicals, the major hyperfine splitting originates from a single α-proton hyperfine coupling and their EIE spectra were also quite similar. The similarity of the EIE spectra and hyperfine tensors led to the assumption that there are only two essentially different radical structures. The radical exhibiting only β-proton hyperfine couplings was assigned to a C3 centered radical arising from H3 abstraction and the other radical suggested to be an open-ring species with a disrupted C2−C3 bond and a double C2−O2 bond. A possible formation mechanism for the latter open-ring radical is presented. By means of cluster density functional theory (DFT) calculations, the structures of the two radicals were determined and a fairly good agreement between the calculated and experimental hyperfine tensors was found.

Introduction

The study of free radical structures and properties is an active research area for experimental as well as for computational research groups. In particular, radicals can be detected by electron paramagnetic resonance (EPR) spectroscopy in aqueous media (e.g., with spin-traps), frozen solutions, dry powders, and single crystals. For many purposes, single crystals are more advantageous because they can provide accurate structural information on radicals and their immediate surroundings. Recent advances in the development of fast computers and efficient algorithms have offered computational groups the ability to calculate complex radical structures in shorter time. In that respect, density functional theory (DFT) has already in many cases proven to be quite adequate in reproducing experimental hyperfine coupling tensors and hence assisting in radical model assignments and structure determinations.[1,2]

A central issue in the radiation chemistry of DNA is the identity and the consequential effects of primary radicals in the 2′-deoxy-D-ribose sugar unit. Irradiation of DNA causes sugar radicals through, e.g., ionization followed by deprotonation at the carbon sites. The relative abundance of sugar radicals in irradiated hydrated DNA was estimated at 12.5%.[3] Despite of this seemingly low abundance, sugar radicals almost invariably lead to strand breaks and when produced on both strands in proximity of each other, they can result in a lethal double-strand break.[3] Strand breaks result from cleavage of the phosphate ester bond at either the 3′ or 5′ ends of the sugar−phosphate backbone. The cleavage of these bonds probably occurs by secondary radical processes after ionization and deprotonation on the DNA sugar.

In the past decade, the disaccharide sucrose has been considered as an emergency EPR-dosimeter for nuclear radiation accidents.[4] Sucrose, better known as table sugar, is a common sweetener present in substantial quantities in most households. When sucrose is exposed to ionizing radiation, relatively stable radicals are formed, which can serve as a probe for estimating radiation doses. However, it is well-known that exposure of carbohydrates to ionizing radiation can lead to a large number of radicals. Also in sucrose, the numerous radicals result in a strongly composite and complex EPR spectrum, which can compromise precise and reliable dose assessments if the radicals have a different dose response. The unambiguous identification of sucrose radicals remains a challenge.[5−7]

In view of the food safety and hygienic quality, β- and γ-radiation treatment of some foodstuffs is a growing practice in many countries. From a regulatory point of view, reliable techniques are needed to discriminate irradiated from nonirradiated food. The application of these techniques by authoritative instances should promote a proper use of radiation in combination with food. One of these techniques is EPR spectroscopy. A huge number of foodstuffs contains carbohydrates and when irradiated exhibit different but characteristic EPR spectra. From a practical point of view, the EPR patterns found in food have to be correctly identified, to detect any sign of radiation treatment and optionally to quantify this radiation dose.

To contribute to the above-mentioned issues, simple molecular model systems, such as glucose,[8] fructose,[9] and sorbose[10,11]

* To whom correspondence should be addressed. Tel: +32 9 264 43 51. Fax: +32 9 264 49 96. E-mail: gauthier.vanhaelewyn@ugent.be.
† Department of Solid State Sciences, Ghent University.
‡ Center for Molecular Modeling, Ghent University.
§ University of Oslo.
# Postdoctoral Fellow of the Fund for Scientific Research − Flanders (Belgium)(F. W. O. − Vlaanderen).

10.1021/jp056632v CCC: $33.50
Published on Web 01/25/2006

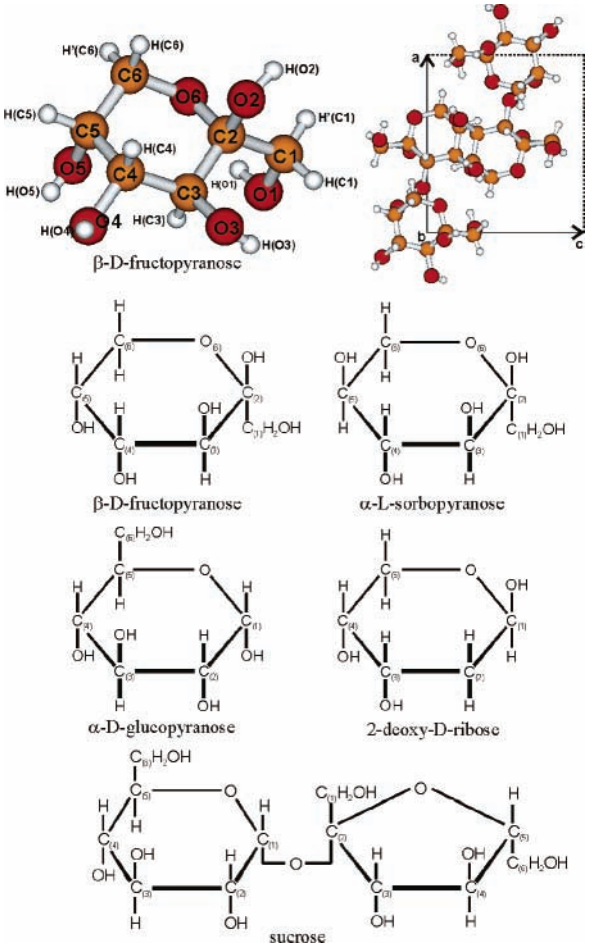

Figure 1. Upper left: molecular structure of β-D-fructose with labeled atoms. Upper right: four β-D-fructose molecules at four different crystallographic sites. Bottom: chemical structures of fructose, sorbose, glucose, deoxyribose, and sucrose for comparison.

(see Figure 1 for the intact molecules and their atom numbering), have previously been studied in the solid state to elucidate the nature and structure of radiation induced sugar radicals. It is worth emphasizing that the molecular structure of fructose in the solid state is in the pyranose form (six ring structure). Some of the radical models proposed in the former references have also been confirmed by comparing the experimental hyperfine tensors with DFT calculated tensors. Most often, these calculations are performed within a single molecule approach, implying that the theoretical model only contains the radical within a vacuum and that no intermolecular interactions between radical and crystal lattice are taken into account. Although the explicit treatment of these interactions has the potential of providing a superior agreement between theory and experiment,[12] sometimes satisfactory results can be obtained with the aid of the computationally less expensive single molecule approximation. For example, in glucose single crystals X-irradiated at 12 and 77 K, the radical models called species **I** (hydrogen abstraction from C6) and **II** (hydrogen abstraction from C3) could convincingly be confirmed with DFT[13] by comparison of both the principal values and directions. In fructose single crystals X-irradiated at room temperature, a radical model with OH abstraction from C2 was tentatively proposed.[14] In sorbose single crystals X-irradiated at room temperature, a radical model resulting from hydrogen abstraction from C3 could be confirmed with DFT[11] by comparison of both the principal values and principal directions. In the latter case, two molecular conformations of the sorbose molecule coexist in the crystal lattice (with slightly different orientations of the C1−O1 bound). Although two, very similar, radical species were resolved experimentally, it was not possible at that time to distinguish between the two structures with single molecule DFT calculations.

Radicals detected at room temperature are usually not the primary radicals formed by direct interaction with radiation. Some of the primary radicals are unstable and act as precursors to secondary radicals. In the process of such radical conversions or reactions, the primary radicals might often be the most important key issues in understanding the ultimate effects of radiation on biological organisms. For example, if the cleavage of the phosphate ester bond that leads to DNA strand breaks is caused by one or more sugar radical precursors, it is of fundamental importance to assess their nature. Creating radiation defects at low temperature (LT) might prevent secondary radical reactions from proceeding and hence make it feasible to study the primary radicals.

A major difference exists between the mechanisms of formation for sugar radicals in the solid state and in liquid solutions.[15] In the latter case, indirect processes, e.g., dehydrogenation at a carbon site by radiation-induced hydroxyl radicals from water radiolysis, is far more important than the direct effect of radiation, that is, ionization and subsequent deprotonation, which are the prominent processes in solids. Therefore, the study of carbohydrates in liquid solutions certainly is important but mostly only complementary to the study of radicals and their formation mechanisms in the solid state.

In this work, single crystals of fructose were irradiated at 80 K and subsequently measured with EPR, electron nuclear double resonance (ENDOR) and ENDOR-induced EPR (EIE) at the same temperature. All experiments were performed with a specially designed Q-band ENDOR cavity, allowing for X irradiation of an oriented single crystal at liquid nitrogen temperatures. Our assumptions for radical models will be supported by DFT calculations.

Materials and Methods

Materials. The β-D-fructose powder was purchased from Aldrich, and single crystals were grown from an aqueous H_2O solution containing ethanol at room temperature.[16] Single crystals with suitable dimensions ($\approx 1 \times 1 \times 2$ mm) were chosen for the experiments. The crystals are orthorhombic with space group $P2_12_12_1$ and four molecules in the unit cell.[17,18] The *a*, *b*, and *c* axes were chosen as a reference axis system for the electron magnetic resonance (EMR) experiments. The axes were labeled according to the neutron diffraction study,[18] i.e., $a = 0.9191$ nm, $b = 1.0046$ nm, and $c = 0.8095$ nm, whereas the atomic coordinates were taken from the X-ray diffraction study[17] because in ref 18 the coordinates refer to the L enantiomer and not the D enantiomer as in β-D-fructose. The fructose molecules are in the pyranose form which is also the crystalline form for e.g. α-D-glucose, α-L-sorbose and 2′-deoxy-D-ribose. In Figure 1, the molecular structure of β-D-fructose based on the data in ref 17 is shown, together with a comparison of its chemical structure with some other structures relevant for this study.

Experimental Methods. Single crystals of β-D-fructose were mounted onto a goniometer head of a Weissenberg X-ray diffraction camera. Using oscillation diagrams, the selected crystal axis was aligned with the rotation axis within 1°. The crystal was then transferred and glued (TraCon silver epoxy) onto the tip of a copper crystal holder mounted to an Air Products coldfinger cryostat without loss of alignment. The cryostat was then inserted into the cryostat holder (vacuum shield) of the Q-band cavity. In this way, the position of the

crystal was adjusted to the same height as the thin (0.2 mm) aluminum irradiation window in the vacuum shield, positioned immediately above the cavity which is operated in the TE_{011} mode. The maximum sample diameter was 4 mm. Before X-irradiation, the crystal holder and crystal were cooled to liquid nitrogen temperature. The X-ray dose delivered to the crystal was estimated to be about 30 kGy. After irradiation, the crystal was carefully lowered into the resonance cavity for EMR measurements.

The Q-band EPR, ENDOR, and EIE experiments were performed using a Bruker ESP300E spectrometer equipped with a Q-band bridge having a maximum microwave power of 150 mW and the DICE ENDOR accessory. For ENDOR and EIE, an ENI 3200L RF power amplifier was used. The microwave frequency was measured using an HP 5324A 40 GHz frequency counter.

The Q-band EPR/ENDOR cavity was specially developed by the EPR group at the University of Oslo for structural studies of radicals in single crystals X-irradiated at low (liquid He or N_2) temperature, and with subsequent EPR/ENDOR/EIE/TRIPLE measurements at the same temperature or at any temperature above the irradiation temperature. EPR and ENDOR measurements were made by rotating the sample in 5° intervals through 180° by simply rotating the cryostat in the cavity holder. The program MAGRES[19,20] was used to derive the hfc tensors from the ENDOR data. A six-parameter linear regression routine generates these tensors from the polar angles (θ,φ) of the rotation axes, the measurement angle α, and the corresponding measured ENDOR frequencies. Refinements including a total of nine angles (θ, φ, and the starting angle α_0 for each plane) were made, using a nonlinear refinement procedure converging to minimum root-mean-square (rms) value for the complete data set. The program KVASAT[21] was used to simulate the single-crystal EPR and EIE spectra. This program includes microwave power saturation effects in an empirical manner. Precise determination of the **g**-tensors was not feasible due to complex EPR spectra and the lack of adequate and well-resolved EIE spectra at magnetic field orientations intermediate to the crystallographic axes.

Computational Details

To aid in the identification of the radical species that were observed in the measurements, high-level DFT calculations were performed on several radical models. A cluster approach was adopted, in which a part of the crystal lattice was explicitly modeled by placing discrete molecules around the target radical, in accordance with the crystal structure. In total, eight fructose molecules, along with the central radical, were taken up in the cluster (see Figure 2). This constitutes the smallest cluster that has any physical significance, since it contains all molecules that are involved in hydrogen bonds with the central fructose unit. Geometry optimizations were then performed on the central radical only, by constraining the atoms of the outer fructose molecules to their original crystallographic coordinates. Although this model space approach poses considerably more demands on computational resources than a single molecule approximation, it is far superior to the latter. In a recent work on glucose radicals,[22] the difference between both approaches was thoroughly assessed and the cluster geometries were found to give far better results when compared to experiment.

After the optimizations, hyperfine coupling tensors were calculated for the optimized radical geometries, still taking into account the surrounding fructose molecules. This also presents a further computational burden, but it has been shown that this procedure results in substantially better calculated hyperfine data.[12,22]

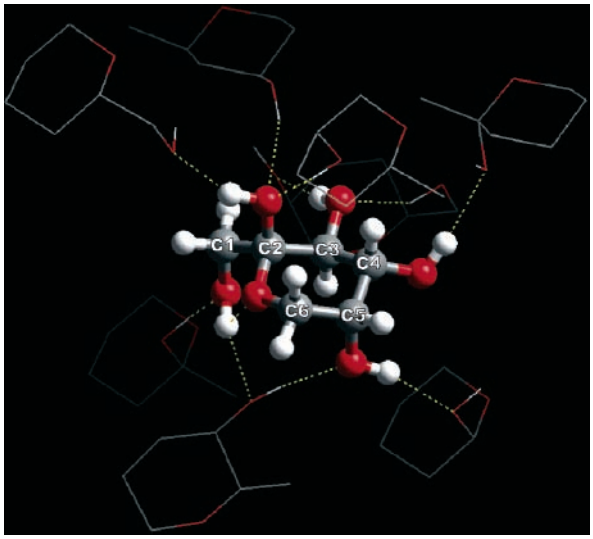

Figure 2. Cluster model structure for the DFT calculations of the β-D-fructose radicals. The central moiety is surrounded by eight fructose molecules.

All calculations were performed with the Gausian03 software package,[23] employing the B3LYP functional[24] along with a triple-ζ 6-311G basis set augmented with single d and p polarization functions (6-311G**).[25,26] This level of theory has proven reliable in earlier computational studies of carbohydrates.[10,13,14]

Results

X irradiation of β-D-fructose single crystals at low temperature without annealing leads to EMR spectra different from the ones previously observed after X irradiation at room temperature[9] where the crystal EPR spectra could roughly be simulated adding two spectral contributions each due to three nonequivalent proton hyperfine couplings. In Figure 3, 77 K EPR spectra obtained for the magnetic field along each of the crystallographic axes are shown, together with EIE spectra obtained by locking the rf-frequency at the ENDOR lines originating from three different radicals. EIE allows the isolation of an EPR spectrum corresponding to a single radical, because for a nucleus with $I = {}^1/_2$, the EIE spectrum is similar to the EPR absorption spectrum.

Altogether, hyperfine tensors assigned to four different radicals could be determined from the ENDOR spectra, henceforth labeled R1, R1′, R2, and R3. ENDOR angular variations were recorded in the three principal crystallographic planes (*ab*, *bc*, and *ca* planes). If sufficient ENDOR data of a specific hyperfine interaction were obtained, its corresponding coupling tensor was determined (Table 1).

The EIE technique helped to identify the origin of the various ENDOR lines. It was thereby revealed that a major radical, denoted R1, exhibits four relatively isotropic protonhyperfine (HF) interactions, more specifically one large (labeled HF1, in the range 94−107 MHz) and three smaller (labeled HF2, HF3 and HF4, in the range 6−25 MHz) interactions. The observed ENDOR lines of the various HF interactions are shown in Figure 4 for the magnetic field direction parallel to the *a*, *b*, and *c* axes. The high-frequency line of the large interaction HF1 was relatively intense and could be observed at all magnetic field orientations. The determination of its tensor easily led to the

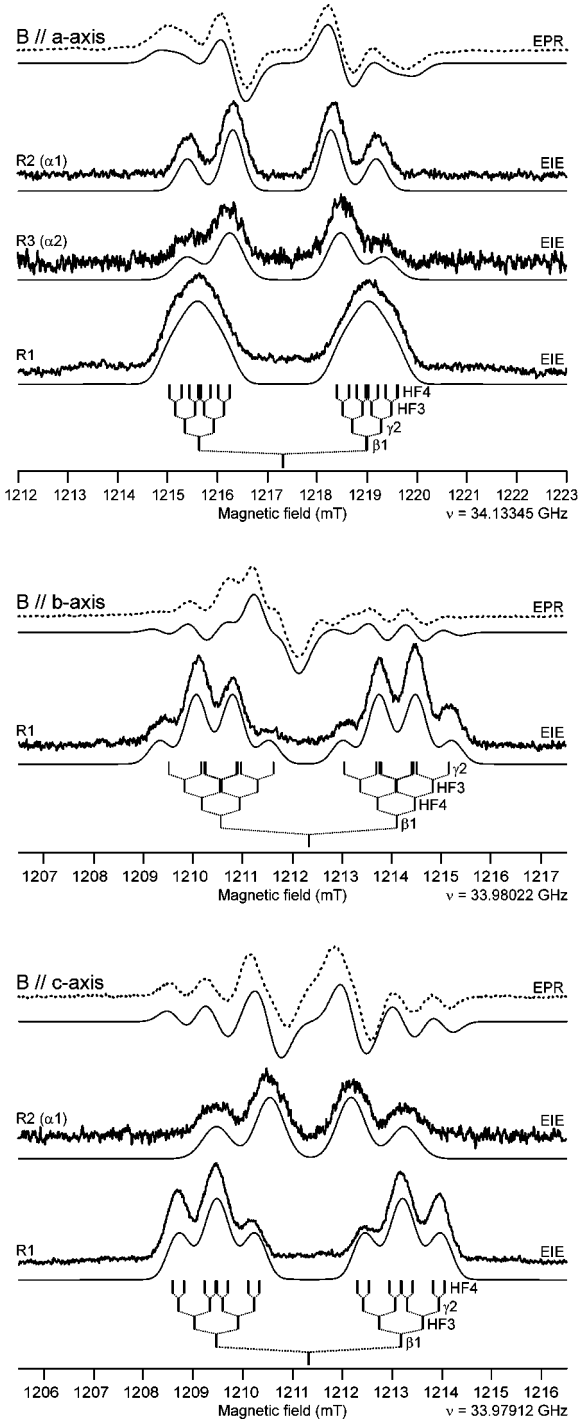

Figure 3. Q-band EPR and EIE spectra of 77 K X-irradiated fructose single crystals measured at 77 K for the magnetic field along the crystallographic axes. Each experimental spectrum is accompanied, immediately below, by its simulation. Underneath the EIE spectrum of radicals R1/R1′, for each crystallographic axis, is a outline of the hyperfine splittings involved based on the ENDOR data for the corresponding axis.

identification of HF1 as a β-coupling, henceforth denoted $\beta 1$ with tensor $\vec{\mathbf{A}}_{\beta 1}$. Only two of the smaller couplings (HF2 and HF4) could satisfactorily be resolved for off-axis orientations and resulted in the tensors $\vec{\mathbf{A}}_{\mathrm{HF2}}$ and $\vec{\mathbf{A}}_{\mathrm{HF4}}$, whereas the third one (HF3) was only observed at the axes. Performing EIE on any one of the ENDOR lines of $\beta 1$, HF2, HF3, and HF4 resulted in the same EIE absorption spectrum as seen in Figure 3 and labeled by R1. Below these EIE spectra is a schematic drawing of the hyperfine splittings caused by $\beta 1$, HF2, HF3, and HF4.

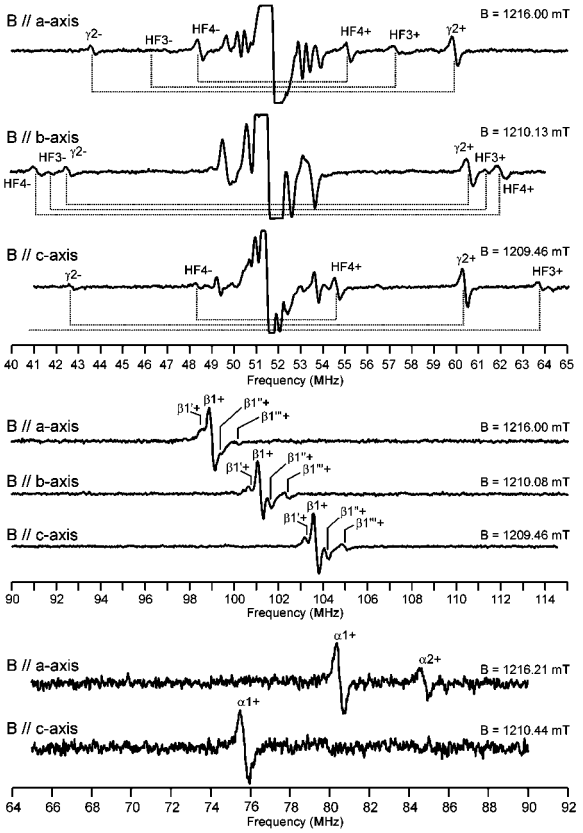

Figure 4. Q-band ENDOR spectra in different frequency ranges from 77 K X-irradiated fructose single crystals measured at 77 K for the magnetic field along the crystallographic axes. The magnitude of the magnetic field is indicated above each ENDOR spectrum and can be linked with the field values of the EPR spectra in Figure 1. The high and low-frequency ENDOR resonances are indicated with superscript + and −, respectively. The first six spectra show the resonances associated with R1 ($\beta 1$, $\gamma 2$, HF3, HF4), R1′ ($\beta 1'$), R1″ ($\beta 1''$), and R1‴ ($\beta 1'''$). The last two spectra show the resonances associated with R2 ($\alpha 1$) and with R3 ($\alpha 2$).

For *B*//*a* axis, HF2, HF3, and HF4 are all different and small (0.58, 0.40, and 0.24 mT, respectively), resulting in a broad doublet ($\beta 1$ gives 3.37 mT); for *B*//*b* axis, HF2, HF3 and HF4 are larger and nearly identical (0.65, 0.70, and 0.75 mT, respectively) resulting in a doublet of quadruplets ($\beta 1$ gives 3.54 mT); for *B*//*c* axis, HF2 and HF3 have similar magnitudes whereas HF4 is clearly smaller (0.64, 0.88, and 0.23 mT, respectively) resulting in a doublet of triplets ($\beta 1$ gives 3.72 mT).

Next to the $\beta 1^+$ resonance line assigned to R1, one can in the ENDOR spectra in Figure 4 see other, much weaker lines. In fact the resonance lines of $\beta 1$ seem in all three rotation planes to be closely accompanied by resonance lines of three other couplings (one slightly smaller and two slightly larger than $\beta 1$) that exhibit an angular variation similar to that of $\beta 1^+$. In practice it was possible to determine only the hyperfine tensor of the coupling (denoted $\beta 1'$) that is slightly smaller than $\beta 1$ (see Table 1). Although both tensors $\vec{\mathbf{A}}_{\beta 1}$ and $\vec{\mathbf{A}}_{\beta 1'}$ appear to be very similar, they are distinct and considering the EPR/EIE spectrum, they can certainly not originate together in the same radical. Hence, we will assume the $\beta 1'$ signal to originate from the radical R1′, and analogously, the resonance lines indicated by $\beta 1''$ and $\beta 1'''$ to originate from R1″ and R1‴, respectively.

As far as one may assume that the ENDOR resonance lines of $\beta 1$, $\beta 1'$, $\beta 1''$, and $\beta 1'''$ are sufficiently separated at certain orientations of the magnetic field, their EIE spectra at these orientations were indistinguishable with respect to their shape.

TABLE 1: Proton Hyperfine Coupling Tensors (MHz) Acquired from Low Temperature Q-band ENDOR Measurements on Low Temperature X-Irradiated β-D-Fructose Single Crystals

					principal directions		
radical	tensor	principal values	isotropic values	anisotropic values	*B*//*a*	*B*//*b*	*B*//*c*
	$\overleftrightarrow{\mathbf{A}}_{HF1(\beta1)}$	106.40 (02)	99.41	7.00	−0.0706 (0011)	0.4709 (0060)	0.8794 (0009)
		97.42 (02)		−1.99	−0.1536 (0007)	−0.8762 (0006)	0.4569 (0054)
		94.40 (02)		−5.01	−0.9856 (0004)	0.1028 (0012)	−0.1342 (0028)
	$\overleftrightarrow{\mathbf{A}}_{HF2(\gamma2)}$	23.49 (03)	17.63	5.86	0.4795 (0018)	−0.6227 (0107)	0.6183 (0068)
		15.35 (03)		−2.29	0.4971 (0014)	0.7734 (0018)	0.3934 (0126)
		14.06 (02)		−3.57	0.7232 (0014)	−0.1187 (0106)	−0.6804 (0051)
R1		11.12 (B//a)					
	$\overleftrightarrow{\mathbf{A}}_{HF3}$	19.68 (B//b)	18.49				
		24.67 (B//c)					
	$\overleftrightarrow{\mathbf{A}}_{HF4}$	21.41 (02)	11.42	10.00	0.1222 (0018)	0.9912 (0027)	−0.0511 (0026)
		7.03 (03)		−4.39	0.7194 (0003)	−0.0530 (0020)	0.6926 (0024)
		5.81 (03)		−5.61	0.6838 (0028)	−0.1214 (0027)	−0.7195 (0026)
R1′	$\overleftrightarrow{\mathbf{A}}_{\beta1'}$	105.53 (02)	98.58	6.95	−0.0795 (0014)	0.4573 (0083)	0.8858 (0018)
		96.70 (03)		−1.87	−0.2143 (0010)	−0.8757 (0013)	0.4328 (0077)
		93.50 (03)		−5.08	−0.9735 (0005)	0.1554 (0019)	−0.1676 (0034)
R2	$\overleftrightarrow{\mathbf{A}}_{\alpha1}$	−9.86 (36)	−38.88	29.03	0.1643 (0027)	0.9312 (0014)	−0.3253 (0053)
		−35.26 (10)		3.63	0.6102 (0024)	−0.3550 (0048)	−0.7083 (0020)
		−71.54 (06)		−32.65	−0.7751 (0020)	−0.0821 (0027)	−0.6265 (0018)
R3	$\overleftrightarrow{\mathbf{A}}_{\alpha2}$	−12.64 (18)	−45.59	32.94	0.3149 (0008)	0.8774 (0010)	−0.3619 (0017)
		−43.92 (09)		1.66	0.5457 (0022)	−0.4793 (0024)	−0.6873 (0013)
		−80.19 (05)		−34.60	−0.7765 (0006)	−0.0189 (0021)	−0.6298 (0024)

Each of the other two radicals mainly exhibits a single α-proton hyperfine interaction. The radicals that exhibit the hyperfine couplings α1 and α2, were denoted R2 and R3, respectively. The intensity of the α-coupling ENDOR resonance lines was in general much weaker than those of the β-couplings as can be observed in the lower part of Figure 4 for *B*//*a* axis and *B*//*c* axis. The spectrum of the α-lines at *B*//*b* axis is not shown because both α-couplings are very small and their ENDOR resonances are masked by the stronger lines in the vicinity of the distant (or free) proton frequency. R2 and R3 exhibit besides their α-coupling also very small β-couplings. However, none of these β-couplings were resolved in the EIE spectra and mainly due to the difficulty in observing them, attempts were not made to determine their ENDOR angular dependence.

The EIE spectra of the α-proton interactions in Figure 3 show in fact four absorption lines where the inner pair of absorption lines are more intense than the outer pair. The two pairs result from the four possible transitions between the ($M_S = {}^1/_2$, $M_I = \pm{}^1/_2$) and ($M_S = -{}^1/_2$, $M_I = \pm{}^1/_2$) energy levels ($S = {}^1/_2$, $I = {}^1/_2$). It can be calculated to first order[27] that at the present Q-band frequencies, the splitting of the inner lines in the EIE spectra nearly matches the hyperfine splitting calculated by means of the observed ENDOR frequency. At Q-band, the intensities of the outer transition lines usually are small. However, the EIE spectra are recorded at high microwave power (34 mW). The outer lines of the quartet power saturates more slowly than the inner lines resulting in an observable quartet at high microwave power (at X-band, the opposite behavior is most commonly observed[28]).

Immediately below each experimental EPR and EIE spectrum in Figure 3, the corresponding simulation is shown based on data in Table 1. The agreement between the experimental EIE spectra and their simulation is quite good, also with respect to the "forbidden" transitions in the case of each of the single α-couplings. The simulation of each EPR spectrum was performed only with R1 and R2 with an average contribution over the three crystallography axes of about 38% and 62%, respectively. In all three cases the simulations of the experimental spectra are quite acceptable. First, this illustrates that R1, R1′, and the other two contributions related to β1″ and β1‴, but also R2 and R3, are so similar that they are not distinguishable in EPR. Second, that the (important) relative amount of R2 together with R3, both exhibiting weak ENDOR, can be established from the EPR spectrum.

Discussion

Tensor Analysis and Radical Model Assignment. To obtain plausible radical models that may explain the observed resonances, the principal axes of the experimental hyperfine coupling tensors were initially compared with parameters derived from the pristine molecular structure. In particular, experimental isotropic β hyperfine coupling values can be compared with the values calculated using the Heller−McConnell relation if the β coupling tensor is due to hyperconjugation[29]

$$a_{iso}^{\beta} = \rho^{\pi}(B_0 + B_2 \cos^2\theta)$$

where ρ^{π} is the spin density of the $2p_z$ lone electron orbital (LEO) on C_α, B_0 is a (small) constant which arises from spin polarization, B_2 is a coefficient reflecting the hyperconjugation (126 MHz for planar alkyl radicals) and θ is the dihedral angle between the LEO and $C_\beta-H_\beta$. Furthermore, the principal directions corresponding to the largest dipolar hydrogen hyperfine coupling can also be compared with directions between hydrogen atoms and carbon (or oxygen) atoms of the pristine molecule.

Several possible radical models can be formed by net abstraction of hydrogen, hydroxyl or hydroxymethyl from the pristine fructose molecule. However, only a limited number of these models represent radical candidates that could be in possible agreement with the observed hyperfine tensors.

Radical Models for R1 and R1′. Radical models that would exclusively account for β interactions are those where a hydrogen atom is abstracted from C3, C4, or C5 (see Figure 1

for the atom numbering scheme), since hydrogen abstraction from C1 or C6 would obviously result in the occurrence of α-couplings. From the three possible carbon abstraction sites, only C3 and C4 remain serious candidates if one takes the eigenvectors for the maximum principal value of $\tilde{\mathbf{A}}_{\beta 1}$ and $\tilde{\mathbf{A}}_{\beta 1'}$ into account. Comparing these with the crystallographic C3−H(C4) ([−0.0542, −0.5920, −0.8041]) and C4−H(C3) ([0.0473, 0.6471, 0.7609]) directions, the smallest angle of deviation is in the range 11−15°. The small differences between these directions can be due to minor displacements or relaxations of the atoms in the radical after disruption of the involved molecular bond or to the inherent limitations of the point-dipole approximation. Furthermore, the directions associated with C3−H(C4) and C4−H(C3) are the only ones which are close to the eigenvectors of the maximum principal values of $\tilde{\mathbf{A}}_{\beta 1}$ and $\tilde{\mathbf{A}}_{\beta 1'}$ if compared with other C···H or C···OH directions within the pristine molecule.

One could hypothesize that the R1 and R1′ radicals have been formed by hydrogen abstraction from the two different carbon locations: one from C3 and the other from C4. Another possibility is that both radicals originate from the same radical model, either by H(C3) or H(C4) abstraction, but have become slightly distinct because of small conformational differences. The dihedral angle between the C3−H(C3) and C4−H(C4) directions as calculated from the pristine fructose molecule, is 2.6°. Roughly assuming that the LEO corresponds to either of the directions, the observed isotropic hyperfine coupling is obtained using the Heller−McConnell relation with $B_0 \approx 0$ MHz and $B_2 \approx 126$ MHz,[8] if $\rho^{\pi} \approx 0.80$.

It is worth mentioning that in α-L-sorbose X-irradiated at room temperature, two C3 carbon-centered radicals formed by H(C3) abstraction were recently identified,[10] differing only slightly in their conformations. In both cases, the unpaired electron from C3 interacts with H(C4) giving rise to an experimental isotropic coupling of about 70 MHz. The direction corresponding to the largest principal value was also found to be very close to the crystallographic C3···H(C4) direction (within about 2.1°). Assuming the LEO direction to be along the C3−H(C3) direction, a dihedral angle of about 4.1° could be calculated which gave rise to an isotropic coupling in close agreement with the one above, if $\rho^{\pi} \approx 0.60$. The higher spin density in fructose compared to the one in sorbose might be due to a more planar conformation at the radical center. On the other hand, the assumption made in the sorbose radical about the direction of the LEO to be close to the direction of the ruptured C3−H(C3) bond might be slightly incorrect.

Also in α-D-glucose X-irradiated at 77 and 12 K, a similar, with respect to the radical site, C3 carbon-centered radical was proposed on the basis of the determination of two β-coupling tensors.[8] Each of the tensors was found to originate from the interaction with the hydrogen atom bonded to the carbon atoms (C2 and C4) next to the radical center. The angles between the direction vectors of the maximum hyperfine coupling of each of the tensors and the C3···H(C2) and C3···H(C4) directions was 13 and 15°, respectively.

Radical Models for R2 and R3. Radical models that only exhibit an α-coupling without any other resolvable (α or β) couplings are more difficult to establish. Considering the similar angular dependence of both reported α-tensors, one can assume that they originate from the same radical model, only differing in conformation.

A radical model exhibiting a single α-coupling can be formed in various ways. One approach is to assume that the ring structure of the radical model remains intact. In this way models with single α-couplings can be formed by abstraction of either H(C1), H′(C1), OH(C3), OH(C4), OH(C5), H(C6), or H′(C6). At 77 K, only H-abstraction radicals are reasonable, as considerable thermal energy usually is required for the removal of more bulky substituents. Nevertheless, radical models formed by OH-abstraction were considered as well but resulted in less satisfactory agreement with the experimental data than the H-abstraction radical models presented below. Another approach is to assume that the ring structure of the radical is disrupted, in that way more complicated radical models can be formed that can exhibit one or more α-couplings. In the case of R1 and R1′, it was not necessary to consider ring opening events because two very plausible radical candidates could straightforwardly be proposed on the basis of the point-dipole approximation. To deduce a plausible α-type radical model (and structure) from the experimental data, at least the following conditions have to be fulfilled:

SCHEME 1. C1-Centered Fructose Radical Model

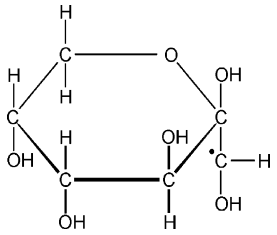

(a) The principal directions of the α-tensor must be in fair agreement with principal directions deduced from the radical structure and in particular, the direction corresponding to the numerically smallest experimental coupling must be in reasonable agreement with a possible C_{α}−H bond direction;

(b) The calculated isotropic hyperfine coupling (using the Heller − McConnell relation) of a β-proton on a neighboring carbon atom must be very small (within the line width);

(c) Considering the close similarity between α1 and α2, the results from parts a and b must provide qualitative agreement for both α-tensors.

By abstraction of a hydrogen atom or by disruption of the ring structure, one can expect that local reorientations of the remaining atoms will take place at the site of disruption and in its vicinity. The final atomic positions of the radical caused by the latter reorientations are, however, difficult to predict and will depend not only on the electronic conformation of the damaged molecule but also on the conformation of its (immediate) environment, especially in the case of disrupted rings.

Possible Radical Models with Intact Ring Structure. Only two plausible radical models with an intact ring structure can be proposed that given rise to a single α-coupling and fulfill conditions a, b, and c.

The first appropriate structure is a hydroxyalkyl radical model centered on C1 (see Scheme 1), resulting from abstraction of either H1 or H1′.

A similar radical was observed in α-D-glucose X-irradiated at 77 and 12 K.[8] Considering the similar chemical composition and structure, along with the comparable irradiation and measurement conditions, it is reasonable to contemplate the formation of this α-proton type radical in fructose. For this purpose, one can assume that the remaining hydrogen atom on C1 relaxes so that it is located on the bisector of the angle defined by O1, C1, and C2 (and hence also in the plane {O1, C1, C2}).[30,31] This atomic rearrangement was later verified in the DFT calculations. Since the eigenvectors in Table 1 only represent one of four possible symmetry related vectors in the

TABLE 2: Proton Hyperfine Coupling Tensors (MHz) from Cluster DFT Calculations for R1 (and R1′) and R2 (and R3)

				principal directions				
radical	tensor	isotropic values	anisotropic values	*B*//*a*	*B*//*b*	*B*//*c*	ψ (°)	ξ (°)
			7.13	−0.0898	0.4928	0.8655	9.3[a]	10.0[b]
	$\overleftrightarrow{\mathbf{A}}_{H4}$	92.45	−2.05	−0.1220	−0.8679	0.4815	15.9[a]	19.6[b]
			−5.08	−0.9885	0.0623	−0.1381	18.3[a]	21.6[b]
			5.51	0.4684	−0.6225	0.6270	0.8[c]	
R1 (R1′)	$\overleftrightarrow{\mathbf{A}}_{H(O2)}$	17.93	−2.11	0.5246	0.7670	0.3695	2.1[c]	
			−3.40	0.7109	−0.1559	−0.6859	2.3[c]	
			21.43	0.4653	0.1000	0.8795		
	$\overleftrightarrow{\mathbf{A}}_{H(O3)}$	9.96	−9.69	−0.6053	0.7609	0.2398		
			−11.73	−0.6458	−0.6411	0.4146		
			37.67	0.2911	0.8989	−0.3275	7.5[d]	2.7[e]
R2 (R3)	$\overleftrightarrow{\mathbf{A}}_{H3}$	−50.44	−1.45	0.5989	−0.4382	−0.6703	5.3[d]	4.0[e]
			−36.22	−0.7460	−0.0011	−0.6659	5.4[d]	2.9[e]

[a] Angles between the principal directions of the experimental tensor $\overleftrightarrow{\mathbf{A}}_{\beta 1}$ and calculated tensor $\overleftrightarrow{\mathbf{A}}_{H4}$. [b] Angles between the principal directions of the experimental tensor $\overleftrightarrow{\mathbf{A}}_{\beta 1'}$ and calculated tensor $\overleftrightarrow{\mathbf{A}}_{H4}$. [c] Angles between the principal directions of the experimental tensor $\overleftrightarrow{\mathbf{A}}_{\gamma 2}$ and calculated tensor $\overleftrightarrow{\mathbf{A}}_{H(O2)}$. [d] Angles between the principal directions of the experimental tensor $\overleftrightarrow{\mathbf{A}}_{\alpha 1}$ and calculated tensor $\overleftrightarrow{\mathbf{A}}_{H3}$. [e] Angles between the principal directions of the experimental tensor $\overleftrightarrow{\mathbf{A}}_{\alpha 2}$ and calculated tensor $\mathbf{A}_{H3}$.

SCHEME 2. C6-Centered Fructose Radical Model

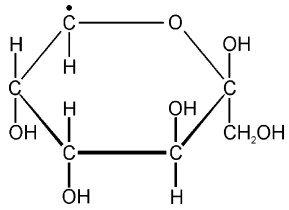

crystal lattice, all possible sign permutations for the direction cosines under the overall orthogonality requirement must be considered.

From the crystallographic data and the α coupling tensors, the angles of deviation between the tensor principal directions (see Table 1) and the expected principal directions can be calculated, based on the proposed radical structure. The deviations corresponding to the numerically minimum, intermediate and maximum hyperfine couplings are 34.8, 56.7, and 59.0° for α1, and 30.5, 58.6, and 62.2° for α2, respectively. These calculated angles in fact represent the overall minimum angle deviations between the tensor principal directions for one of the four different molecule sites and directions associated with the proposed planar radical center.

One complication in this connection is that the coupling tensors $\overleftrightarrow{\mathbf{A}}_{\alpha 1}$ and $\overleftrightarrow{\mathbf{A}}_{\alpha 2}$ in Table 1 are both characteristic for a slightly nonplanar radical center. Thus, the isotropic values[32] indicates LEO spin densities about 25% smaller than those indicated from the dipolar coupling tensor principal elements.[33,34] On the other hand, this nonplanarity (of the order of 10° [34]) is not sufficient to remedy the large angles of deviations above, which in our opinion are too large to lend support to this radical model and structure.

The second structure that could be suitable is a C6-centered radical model (see Scheme 2), generated by abstraction of either H6 or H6′. This model is attractive as some bending at the radical center would be expected, partly due to the closed ring structure and partly since an ester oxygen is the nearest neighbor, which commonly prevents complete planarization of radical fragments of this type.[35,36]

The crystallographic C6−H/C6−H′ bond directions are (−0.139, 0.9840, 0.112) and (0.9783, −0.179, 0.105), respectively. First assuming that the broken C6−H or C6−H′ bond represent the direction of the LEO, the smallest angles of deviation (choosing eigenvector signs similar to those of the crystallographic bond directions) with the eigenvector for the intermediate principal value are 59.1 and 42.7° with respect to the C6−H and C6−H′ bond directions, respectively (Figure 1). On the other hand, if the nonabstracted C6−H fragment remains unchanged in direction, the minimum deviation between the C6−H bond and the eigenvector for the numerically minimum principal value becomes 12.7°. Erling and Nelson[34] showed that in bent α-proton radical fragments, the vector associated with the most-positive dipolar component indicates the direction of the C−H bond and hence that the orthogonal vector associated with the near-zero component of the dipolar coupling, traditionally associated with the direction of the LEO in a planar fragment, will remain perpendicular to the C−H bond and will no longer represent the direction of the LEO. However, we have not been able to envisage a partly relaxed C4−C5−C6(H)−O6−C2 radical structure where the C6−H bond retains its original direction AND the hypothetical direction for the near-zero dipolar coupling is in acceptable agreement with the eigenvector for the intermediate principal value.

Second, assuming that the C5−C6(H)−O6 fragment is planar so that the C6−H bond moves to become located along the internal bisector defined by C5, C6, and O6, the smallest angle of deviation between this direction (choosing eigenvector signs similar to those of the calculated bond direction) with the eigenvector for the numerically minimum principal value becomes 35.9°. The smallest deviation for the eigenvector for the intermediate principal value with the perpendicular to the C5−C6−O6 plane is 46.8°. These deviations are in our opinion too large to support this radical model and structure.

Since the agreement of the previous two models with experimental results is poor, other radical models must be considered.

Plausible Radical Models with Disrupted Ring Structures. Radicals in which the ring structure has been disrupted will have considerably more degrees of freedom than radicals with intact ring structures. As a result, the final conformation for such a radical will predominantly be determined by its interactions with neighboring molecules in the crystal lattice. In addition, it can in most cases be expected that the conformational change with respect to the pristine molecular structure will be quite drastic. This renders the analysis using the point-dipole approximation based on the crystalline atomic coordinates relatively nondiscriminating. Hence, a more objective and systematic approach is required to deduce conceivable radical structures. Theoretical

calculations based on DFT offer this possibility as they allow the determination of the optimal conformation for a model radical within a simulated crystal environment. In addition, these calculations can also resolve several of the ambiguities that were encountered in the discussion on the R1/R1′ radical models.

DFT Calculations of Hyperfine Coupling Tensors. As outlined in the Method section, DFT cluster optimizations were performed on several radical models with intact as well as disrupted ring structures. Since interactions of the induced radical with the crystalline environment are of the utmost importance—especially when the pyranose ring is destroyed—this can best be accomplished by means of cluster calculations. Subsequently the hyperfine coupling tensors were calculated, to find radical structures that could reconstruct the experimental hyperfine tensors.

To discriminate between the different possibilities with respect to the radical candidates for R1 and R1′, cluster calculations were performed on the proposed C3- and C4-centered radicals. By comparing the calculated hyperfine tensors for both structures with the measured $\vec{\vec{A}}_{\beta 1}$ and $\vec{\vec{A}}_{\beta 1'}$ tensors from Table 1, it became apparent that the C4-centered radical cannot possibly account for either of the measured tensors. Instead, both R1 and R1′ originate from the same radical model, obtained by hydrogen abstraction from C3. The optimized geometry for this radical model is illustrated in Figure 5 and the computed hyperfine tensors are presented in Table 2. It is clear that the isotropic and anisotropic couplings reproduce quite satisfactorily the experimental values. In addition, the hyperfine tensor principal directions are also close to the experimental ones, as indicated by the relatively low deviation angles (below 20°). In particular, the calculated H4 hyperfine tensor is in good agreement with $\vec{\vec{A}}_{\beta 1}$ as well as with $\vec{\vec{A}}_{\beta 1'}$. The agreement is even excellent between the H(O2) tensor and $\vec{\vec{A}}_{HF2}$, which further corroborates the assignment of R1 (and R1′) to the proposed C3-centered radical and identifies HF2 as a γ-coupling, henceforth denoted $\gamma 2$ with tensor $\vec{\vec{A}}_{\gamma 2}$. Unfortunately, the coupling tensors for HF3 and HF4 cannot be matched unequivocally. The $\vec{\vec{A}}_{HF3}$ signal can be tentatively assigned to the H(O3) proton, even though a substantially smaller isotropic coupling constant is calculated. Deuteration of the hydroxyl groups may clarify the uncertainty in the latter assignment, however, sufficiently large partially deuterated fructose single crystals have so far not been obtained. No proton coupling tensor could be found in the proposed radical model to match with the measured $\vec{\vec{A}}_{HF4}$. This interaction is most likely due to a hydroxyl proton—relatively far (i.e., γ or even δ position) from the unpaired electron on C3—which takes on a specific orientation under the (weak) influence of neighboring lattice molecules. Presumably, this exact conformation has not yet been attained in the computational model since the constraint was imposed that the molecular environment of the radical cannot change in conformation. Therefore, to adequately reproduce these hyperfine tensors, additional calculations should be performed in which conformational changes in the direct environment of the radical are taken into account. Given the similarity of the R1 and R1′ hyperfine data, a further differentiation between the precise conformations of these radicals is virtually impossible based solely on the $\vec{\vec{A}}_{\beta 1}$ and $\vec{\vec{A}}_{\beta 1'}$ hyperfine coupling tensors.

The optimization of the proposed radical models for R2/R3 with an undisrupted ring did not result in a satisfactory reproduction of any of the two observed α-coupling tensors, as anticipated above. On the other hand, it was found that the radical with a disrupted C2−C3 bond, exhibiting the radical center at C3 and a double bond between C2 and O2, yielded an

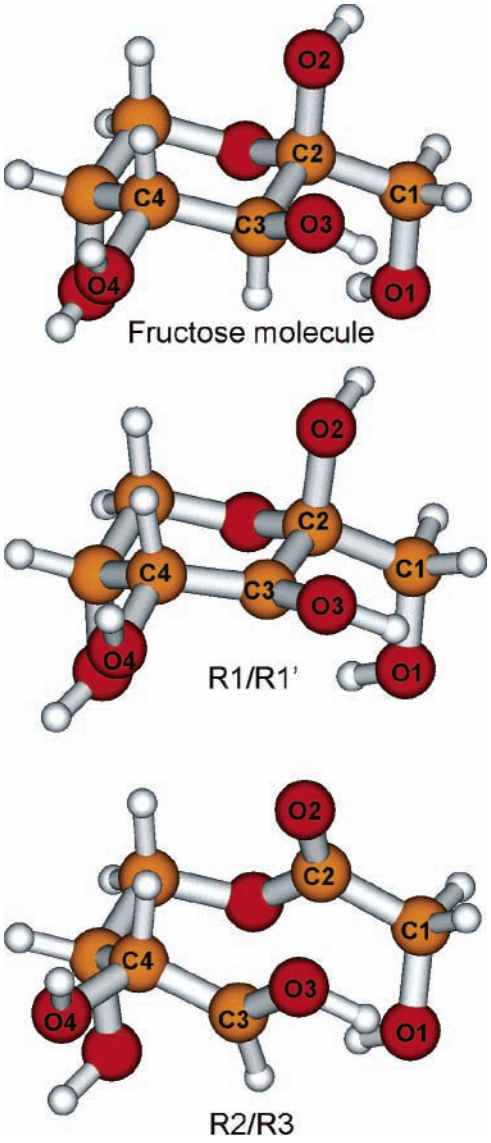

Figure 5. Comparison between the pristine molecular structure (top) and the optimized radical structures for R1/R1′ (middle) and R2/R3 (bottom). Neighbor fructose molecules have been left out for clarity.

α-proton hyperfine coupling tensor with eigenvectors in good agreement with the two experimental α-coupling tensors. However, a discrepancy between the experimental and calculated hyperfine principal values is evident, especially for $\vec{\vec{A}}_{\alpha 1}$ (Table 2). This can in fact be used as an argument against this radical model. In particular, the experimentally observed bending at the radical center is only partly reproduced by the calculations as can be suggested from the comparison between the calculated and experimental principal values (Tables 1 and 2). A possible explanation for this discrepancy is that bending of the radical center in the calculated radical structure could not be fully modeled, maybe due to the limited number of neighbor molecules or the fixed atom positions of the neighboring molecules. The strongest argument in favor of the proposed radical model with the C2−C3 bond disruption is the very good agreement between the experimental and calculated hyperfine principal directions and the fact that these directions are far less sensitive to bending of the radical center.[34] Radicals with a disrupted ring have, however, only scarcely been convincingly identified and modeled in the solid state.

A plausible mechanism for the formation of the open ring radical at 77 K is shown in Scheme 3. This mechanism involves

SCHEME 3. Plausible Mechanism for the Formation of the Open Ring Radical

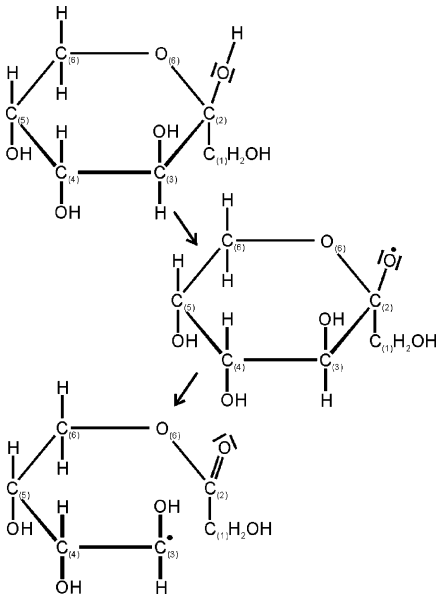

the oxidation of the hydroxyl group on C2 followed by a deprotonation of $H(O2)^+$ resulting in the alkoxyl radical $-C2-O2^{\bullet}$. Such alkoxyl radicals are very common in carbohydrate systems and are commonly observed after LT X irradiation.[37,38] Finally, an electronic reorganization occurs resulting in the C2−C3 bond cleavage, the formation of a carbonyl at C2 and an unpaired electron on C3. Our DFT calculations have shown that this reorganization is exothermic, proceeds without any energy barrier (no activation energy), and thus will be a spontaneous process.

The radical structure R2/R3 differs from the proposed ring-opened radical structure formed in a radiation-induced chain reaction in D-fructose in the solid state.[39] The initial radical species in this chain reaction is a C5-centered radical resulting from H5-abstraction. This radical undergoes an electronic reorganization resulting in a ring-opened species with radical center remaining at C5 ($-{}^{\bullet}C_{(5)}H_2$) that would exhibit two α-couplings. Clearly, however, neither of these two (opened-ring and intact ring) C5 radicals are observed in the present study.

An alternative pathway for ring-opened radicals is to consider radical formation by water elimination. Although this process is most relevant in liquid solutions, it has been shown to occur in the solid state.[40] In the latter study, the water elimination process was observed as a gradual change of the EPR spectrum with time only above 100 K. The process hence requires activation energy. In the present work, no change in the EPR as well as in the ENDOR spectra was observed with time at 80 K. Thus, either the ring opening occurs via a process different from water elimination, or the water elimination process occurs at temperatures below 80 K, which is considered unlikely. The proposed ring opening reaction mechanism in the present study involves only an electronic reorganization and requires no activation energy.

A comparison between the optimized radical structures for R1/R1′ and R2/R3 and the pristine molecule structure, where the neighboring molecules have been left out for clarity, is shown in Figure 5. It can be noticed that for R1/R1′ the radical center at C3 has become more planar, also the atoms O3, H(O3) and H(O1) are also noticeably displaced with respect to their original positions. For R2/R3 large atomic displacements have taken place for C2, O2, C3, O3, C4, and O4 with respect to their original positions. It is worth emphasizing that the current results could only be obtained through cluster DFT calculations, since the $C2-O2^{\bullet}$ alkoxy radical corresponds to a minimum within the single molecule approach.

In a previous paper[9] a radical model (OH abstraction from C2) was suggested in room temperature X-irradiated fructose. This tentative model was established based on a comparison of the principal values and the relative angles between the principal directions between experimental and single molecule DFT calculated hyperfine tensors. As shown previously,[10,13] however, single-molecule DFT calculations may be inadequate for this purpose. Therefore, this assignment should be validated using a new and more sophisticated analysis including cluster DFT calculations.

Summary and Conclusions

A fairly good agreement between the experimental and theoretical hyperfine tensors of the two proposed radical models R1/R1′ and R2/R3 was found by means of cluster DFT calculations. In particular, the open ring radical model R2/R3 could only be obtained by optimizing it inside a cluster of neighbor molecules. The radical model R1/R1′ is equivalent to a radical model that was proposed in X-irradiated sorbose and also similar to a radical model proposed in X-irradiated glucose and the assignment must be considered as strong. The more tentative assignment of the open ring radical model R2/R3 was mainly based on the very good agreement between the experimental and calculated tensor principal axes. The discrepancy between the experimental and calculated principal values may be an indication that the bending at the radical center is possibly not fully modeled by the current cluster DFT calculations.

Acknowledgment. G.C.A.M.V. wishes to acknowledge the Fund for Scientific Research−Flanders (Belgium) (F.W.O.-Vlaanderen) and the Ghent University for the Exploring European Research project (VEO), for the financial support concerning the stay at the University of Oslo.

References and Notes

(1) De Proft, F.; Pauwels, E.; Lahorte, P.; Van Speybroeck, V.; Waroquier, M.; Geerlings, P. *Magn. Reson. Chem.* **2004**, *42*, S3.

(2) Wetmore, S. D.; Boyd, R. J.; Eriksson, L. A. *J. Phys. Chem. B* **1998**, *102*, 7674.

(3) Sevilla, M. D.; Becker, D. ESR Studies of Radiation Damage to DNA and Related Biomolecules. Chapter 6 In *Electron Paramagnetic Resonance: Volume 19*; Specialist Periodical Reports. Royal Society of Chemistry: London, 2004.

(4) Da Costa, Z. M.; Pontuschka, W. M.; Campos, L. L. *Appl. Radiat. Isot.* **2005**, *62* (2), 331.

(5) Gräslund, A.; Löfroth, G. *Acta Chem. Scand. B* **1975**, *29*, 475.

(6) Sagstuen, E.; Lund, A.; Awadelkarim, O.; Lindgren, M.; Westerling, J. *J. Phys. Chem.* **1986**, *90*, 5584.

(7) Vanhaelewyn, G.; Sadlo, J.; Callens, F.; Mondelaers, W.; De Frenne, D.; Matthys, P. *Appl. Radiat. Isot.* **2000**, *52*, 1221.

(8) Madden, K. P.; Bernhard, W. A. *J. Phys. Chem.* **1979**, *83*, 2643.

(9) Vanhaelewyn, G. C. A. M.; Lahorte, P. G. A.; De Proft, F. J. A.; Geerlings, P. F. C.; Mondelaers, W. K. P. G.; Callens, F. J. *Phys. Chem. Chem. Phys.* **2001**, *3*, 1709.

(10) Vanhaelewyn, G. C. A. M.; Jansen, B.; Pauwels, E.; Sagstuen, E.; Waroquier, M.; Callens, F. J. *J. Phys. Chem. A* **2004**, *108*, 3308.

(11) Vanhaelewyn, G. C. A. M.; Jansen, B.; Callens, F. J.; Sagstuen, E. *Radiat. Res.* **2004**, *162*, 96.

(12) Pauwels, E.; Van Speybroeck, V.; Waroquier, M. *J. Phys. Chem. A* **2004**, *108*, 11321.

(13) Pauwels, E.; Van Speybroeck, V.; Vanhaelewyn, G.; Callens, F.; Waroquier, M. *Int. J. Quantum Chem.* **2004**, *99*, 102.

(14) Pauwels, E.; Lahorte, P.; Vanhaelewyn, G.; Callens, F.; De Proft, F.; Geerlings, P.; Waroquier, M. *J. Phys. Chem. A* **2002**, *106*, 12340.

(15) Von Sonntag, C. *The Chemical Basis of Radiation Biology*; Taylor & Francis: London, New York, and Philadelphia, PA, 1987.

(16) Flood, A. E.; Johns, M. R.; White, E. T. *AIChE J.* **2000**, *46*, 239.
(17) Kanters, J. A.; Roelofsen, G.; Alblas, B. P.; Meinders, I. *Acta Crystallogr. B*, **1977**, *33*, 665.
(18) Takagi, S.; Jeffrey, G. A. *Acta Crystallogr. B*, **1997**, *33*, 3510.
(19) Nelson, W. H. *J. Magn. Reson.* **1980**, *38*, 71.
(20) Sørnes, A. R.; Sagstuen, E.; Lund, A. *J. Phys. Chem.* **1995**, *99*, 16867.
(21) Sagstuen, E.; Hole, E. O.; Haugedal, S. R.; Lund, A.; Eid, O. I.; Erickson, R. *Nukleonika* **1997**, *42*, 353.
(22) Pauwels, E.; Van Speybroeck, V.; Waroquier, M. *Spectrochim. Acta A* **2006**, in press.
(23) Frisch, M. J.; Trucks, G. W.; Schlegel, H. B.; Scuseria, G. E.; Robb, M. A.; Cheeseman, J. R.; Montgomery, J. A.; Vreven, T., Jr.; Kudin, K. N.; Burant, J. C.; Millam, J. M.; Iyengar, S. S.; Tomasi, J.; Barone, V.; Mennucci, B.; Cossi, M.; Scalmani, G.; Rega, N.; Petersson, G. A.; Nakatsuji, H.; Hada, M.; Ehara, M.; Toyota, K.; Fukuda, R.; Hasegawa, J.; Ishida, M.; Nakajima, T.; Honda, Y.; Kitao, O.; Nakai, H.; Klene, M.; Li, X.; Knox, J. E.; Hratchian, H. P.; Cross, J. B.; Bakken, V.; Adamo, C.; Jaramillo, J.; Gomperts, R.; Stratmann, R. E.; Yazyev, O.; Austin, A. J.; Cammi, R.; Pomelli, C.; Ochterski, J. W.; Ayala, P. Y.; Morokuma, K.; Voth, G. A.; Salvador, P.; Dannenberg, J. J.; Zakrzewski, V. G.; Dapprich, S.; Daniels, A. D.; Strain, M. C.; Farkas, O.; Malick, D. K.; Rabuck, A. D.; Raghavachari, K.; Foresman, J. B.; Ortiz, J. V.; Cui, Q.; Baboul, A. G.; Clifford, S.; Cioslowski, J.; Stefanov, B. B.; Liu, G.; Liashenko, A.; Piskorz, P.; Komaromi, I.; Martin, R. L.; Fox, D. J.; Keith, T.; Al-Laham, M. A.; Peng, C. Y.; Nanayakkara, A.; Challacombe, M.; Gill, P. M. W.; Johnson, B.; Chen, W.; Wong, M. W.; Gonzalez, C.; Pople, J. A. *Gaussian 03*, Revision B.03, Gaussian, Inc.: Wallingford CT, 2004.
(24) Becke, A. D. *J. Chem. Phys.* **1993**, *98*, 5648.
(25) Krishnan, R.; Binkley, J. S.; Seeger, R.; Pople, J. A. *J. Chem. Phys.* **1980**, *72*, 650.
(26) Mclean, A. D.; Chandler, G. S. *J. Chem. Phys.* **1980**, *72*, 5639.
(27) Miyagawa, I.; Gordy, W. *J. Chem. Phys.* **1960**, *32*, 255.
(28) Sagstuen, E.; Lund, A.; Itagaki, Y.; Maruani, J. *J. Phys. Chem. A* **2000**, *104*, 6362.
(29) Heller, C.; McConnell, H. M. *J. Chem. Phys.* **1960**, *32*, 1535.
(30) Huttermann, J.; Haindl, E.; Schmidt, G.; Bernhard, W. *Int. J. Radiat. Biol.* **1977**, *32*, 431.
(31) Close, D. M.; Nelson, W. H.; Sagstuen, E.; Hole, E. O. *Radiat. Res.* **1994**, *137*, 300.
(32) McConnell, H. M.; Chesnut, D. B. *J. Chem. Phys.* **1958**, *28*, 107.
(33) Bernhard, W. A. *J. Chem. Phys.* **1984**, *81*, 5928.
(34) Erling, P. A.; Nelson, W. H. *J. Phys. Chem. A* **2004**, *108*, 7591.
(35) Sørnes, A. R.; Sagstuen, E. *J. Phys. Chem.* **1995**, *99*, 16857.
(36) Sanderud, A.; Sagstuen, E. *J. Phys. Chem.* **1996**, *100*, 9545.
(37) Box, H. C.; Freund, H. G.; Budzinski, E. E. *J. Chem. Phys.* **1981**, *74*, 2667.
(38) Box, H. C.; Budzinski, E. E. *J. Chem. Phys.* **1982**, *76*, 5645.
(39) Kawakishi, S.; Kito, Y.; Namiki, M. *Agr. Biol. Chem.* **1975**, *39*, 1897.
(40) Samskog, P. O.; Lund, A.; Nilsson, G.; Symons, M. C. R. *Chem. Phys. Lett.* **1979**, *66* (1), 199.